Tandem Site and Size Controlled Pd Nanoparticles for the Directed Hydrogenation of Furfural

Scott M. Rogers,[1,2] C. Richard. A. Catlow,[1,2,5] Carine E. Chan-Thaw,[3] Arunabhiram Chutia,[1,2] Nan Jian,[4] Richard E. Palmer,[4] Michal Perdjon,[1,2,5] Adam Thetford,[1,2] Nikolaos Dimitratos,[1,5] Alberto Villa,[*1,3] and Peter P. Wells[*1,2,6,7]

[1.] UK Catalysis Hub, Research Complex at Harwell, Rutherford Appleton Laboratory, Harwell Oxon, Didcot, OX11 0FA, UK.

[2.] Department of Chemistry, University College London, 20 Gordon Street, London, WC1H 0AJ, UK.

[3.] Dipartimento di Chimica, Università degli Studi di Milano, via Golgi 19, 20133 Milano, Italy.

[4.] Nanoscale Physics Research Laboratory, School of Physics and Astronomy, University of Birmingham, Edgbaston, Birmingham, B15 2TT, UK.

[5.] Cardiff Catalysis Institute, School of Chemistry, Cardiff University, Cardiff, CF10 3AT, UK.

[6.] Diamond Light Source, Harwell Science and Innovation Campus, Chilton, Didcot, OX11 0DE, UK.

[7.] School of Chemistry, University of Southampton, Highfield, Southampton, SO17 1BJ, UK.

ABSTRACT: The conversion of biomass to useful chemical products requires precise catalytic properties to achieve the required activity, selectivity and durability. Here we show, through optimized colloidal-synthesis, the tandem control of Pd size and site availability for the directed hydrogenation of the bio-derived intermediate, furfural. Adjusting the temperature of colloidal reduction dictates the size of Pd nanoparticles; in some instances ultra-small clusters <20 atoms are achieved. Whereas, changing the solvent-system, affects the PVA-Pd interaction and relative proportion of available surface-sites (corners, edges, planes), allowing us to control the selectivity to the valuable hydrogenation products of furfuryl alcohol and tetrahydrofurfuryl alcohol. We demonstrate, through combined experimental and computational studies, that Pd nanoparticle planes are more prone to deactivation through the formation of Pd carbide, and the resulting reduced efficacy of furfural binding. This approach to nanoparticle optimization is an important strategy for producing long-lasting, high-performance catalysts for emerging sustainable technologies.

Keywords: Pd nanoparticles, Colloids, Clusters, Furfural hydrogenation, Heterogeneous catalysis, Pd carbide

Introduction

Upgrading biomass to useful products, be it energy or platform intermediates, is a crucially important part of a sustainable chemicals industry. The hydrolysis of hemicellulose is one example, where one of the major products, xylose, is acid catalyzed to the valuable intermediate furfural.[1-2] Furfural is readily valorized, and is an important precursor in the generation of biofuels[3-4] and chemical intermediates.[2] Furfuryl alcohol, used in the manufacture of resins, adhesives, and synthetic fibres,[5] is produced from the selective hydrogenation of furfural. Subsequent hydrogenation of furfuryl alcohol produces tetrahydrofurfuryl alcohol, a 'green solvent', often used in printer inks and agricultural applications.[6] Ultimately, the hydrogenation of furfural results in a complex network of products (Figure 1), where there is a need to control the relative distribution. The challenge is to find a selective catalyst that has control over C=C or C=O hydrogenation and disfavors alternative pathways, e.g. decarbonylation.

Many heterogeneous catalysts have been investigated for the hydrogenation of furfural, with the majority of studies focusing on Cu, Ni,[7] Ru,[8] or Pd[9-10] based systems. Cu, in the form of Cu chromite,[11] or supported forms,[12-15] have been commonly used, and show good selectivity to furfuryl alcohol as a consequence of the preference of Cu to bind C=O, over C=C.[15] Ni catalysts show different product distribution to Cu, with the primary step favoring decarbonylation, with secondary paths including opening of the furan ring.[16] Pd is an ideal catalyst for hydrogenation processes as it readily dissociates hydrogen under ambient conditions. Recent studies have shown that Pd/TiO_2 based systems are able to effectively hydrogenate furfural and furfuryl alcohol at mild conditions (room temperature, 1-3 bar hydrogen).[17-19] The studies focused on Pd nanoparticles prepared by incipient wetness impregnation and showed that methyl furan and furfuryl alcohol were the major products and that the product distribution could be altered by changing the solvent of reaction and metal loading.[17] Indeed, the differences in furfural binding (η^1 CO, η^1 O, η^2 C-

O, and η^2 C-C) and their preference on specific crystal facets,[20-21] have been linked to variations in product selectivity for different particle sizes.[22] As well as particle size effects, the ability to manipulate the binding orientation of furfural on to specific metal sites, to selectively control the hydrogenation pathway, has been effectively achieved using self-assembled monolayers (SAMs) as blocking agents.[23-25] Medlin *et al.* used thiolates to selectively block facets, leaving only particles edges/corners exposed.

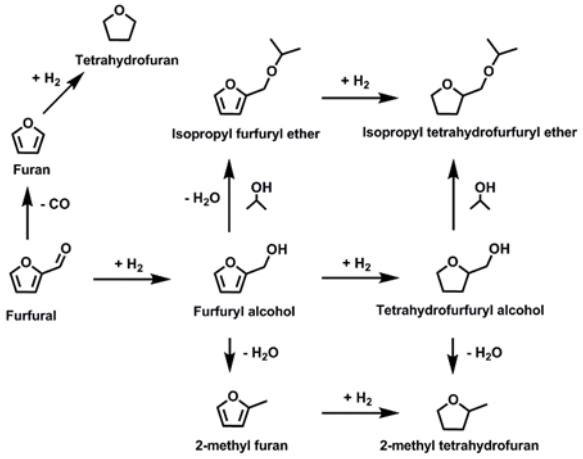

Figure 1. Schematic representation of reaction pathways during furfural hydrogenation.

In this study, we report for the first time, how Pd/TiO_2 catalysts prepared through controlled sol-immobilization routes,[26] affords series of nanoparticles of tailored particle size distributions, including populations of metal clusters. We show, systematically, how particle size and the solvent system of preparation influences the activity, selectivity and stability of the catalysts during furfural hydrogenation at mild reaction conditions of 25 and 50°C. Furthermore, we demonstrate changes to the nanoparticle structure, through carbidization, which causes catalyst deactivation. To our knowledge, this is the first time this deactivation route has been reported.

Methods.

Catalyst Preparation. Supported Pd NPs were prepared using a standard sol-immobilisation method with temperature control during the reduction process. K_2PdCl_4 was used to prepare solutions with various H_2O/EtOH ratios of the desired palladium concentration (1.26 x 10^{-4} M), to which aqueous solutions of PVA (PVA/Pd (wt/wt) = 0.65) were added. 0.1 M solutions of $NaBH_4$ ($NaBH_4$/Pd (mol/mol) = 5) were freshly prepared in the respective solvent and added drop-wise to each solution over a one minute period with stirring to form dark brown/black sols. After the complete reduction of Pd species, 30 minutes, the colloidal solution was individually immobilized on TiO_2 (commercial P25) under vigorous stirring conditions. The amount of support material required was calculated so as to give a final metal loading of 1 wt. %. The mixture was acidified to pH 1-2 by sulfuric acid before stirred for 60 minutes to accomplish full immobilization of the metal NPs on to the support. The slurry was filtered, washed thoroughly with distilled water, and dried overnight at room temperature.

Transmission Electron Microscopy (TEM) and High Angle Annular Dark Field Scanning TEM (HAADF STEM) Imaging. Samples for examination by TEM and aberration-corrected HAADF STEM were prepared by first dispersing the catalyst powder in high purity ethanol using ultra-sonication for 30 minutes. 40 µL of the suspension was dropped on to a holey carbon film supported by a 300 mesh copper TEM grid before the solvent was evaporated. A JEOL JEM 2100 EM was used for HAADF STEM analysis at the Nanoscale Physics, Chemistry and Engineering Research Laboratory at the University of Birmingham by using a JEOL JEM2100F STEM equipped with a spherical aberration corrector (CEOS). The HAADF detector was operated with an inner angle of 62 mrad and an outer angle of 164 mrad. The integrated HAADF STEM intensity analysis was used to obtain the size of ultrasmall clusters, with large Pd clusters functioning as mass balances.[27-28] The 3D intensity plot of the small Pd clusters was performed using the imagej software.

Infra-red CO chemisorption studies. Fourier transform infra-red (FTIR) transmission spectra were obtained with is10 Nicolet spectrometer at a spectral resolution of 2 cm^{-1} and accumulating up to 64 scans. For each experiment, ~25 mg catalyst was pressed to form a very thin pellet. The cell was purged with helium for 30 minutes to obtain a background spectrum before CO was introduced using a 10 % CO/He mixture at 70 mL min^{-1} over a 30 second period. Three CO doses of this nature were administered for each experiment. The gas was switched to helium for 30 minutes at 70 mL min-1, in order to remove gaseous and physisorbed CO before obtaining a spectrum.

X-ray Absorption Fine Structure (XAFS). XAFS studies were performed to examine the Pd oxidation state (XANES) as well as the average Pd particle size from the primary shell coordination number (EXAFS). Pd K-edge XAFS studies were carried out on the B18 beamline at the Diamond Light Source, Didcot, U.K. Measurements were performed in transmission mode using a QEXAFS set-up with a fast-scanning Si(311) double crystal monochromator and ion chamber detectors. The time resolution of the spectra was 1 min/spectrum (k_{max}=18). On average, 15 scans were acquired to improve the signal-to-noise level of the data. XAS data processing was performed using the Demeter IFEFFIT package. [29-30]

Catalytic studies. Furfural hydrogenation was performed at 25 or 50°C, using a stainless steel reactor (30 mL capacity), equipped with heater, mechanical stirrer, gas supply system and thermometer. Furfural solution (15 mL; 0.3 M in 2-propanol) was added into the reactor and the desired amount of catalyst (Furfural/metal ratio=500 mol/mol) was suspended in the solution. The pressure of the hydrogen was 5 bar. The mixture was let at room temperature (25°) or in alternative heated 50°C and mechanically stirred (1250 rpm). At the end of the reaction, the autoclave was cooled down to room temperature (when performed at

50°C), H_2 flow stopped and the autoclave purged with flowing nitrogen. Samples were removed periodically (0.2 mL) and HP 7820A gas chromatograph equipped with a capillary column HP-5 30m x 0.32mm, 0.25 µm Film, by Agilent Technologies. Authentic samples were analyzed to determine separation times. Quantitative analyses with external standard method (n-octanol) was used.

DFT studies. The Vienna Ab-initio Simulation Package (VASP) was used to perform DFT based calculations with Grimme's D2 corrections.[31-35] The projector augmented wave (PAW) method was used and the cut-off energy for the expansion of the plane-wave basis set was set to 550eV, which gave bulk energies converged to within 10E– 5 eV. A convergence criterion of 0.01 eV/Å for our structural optimizations was adopted. For all the preliminary calculations, the most commonly used Perdew-Burke-Ernzerhof (PBE) version of the generalized gradient approximation (GGA) was used to carry out total energy calculations and perform geometry optimizations.[36] For the bulk calculations, the Brillouin zone was integrated using a Monkhorst-Pack (MP) grid of 11×11×11 k-points. Since it is known that the Pd(111) surface is the most stable surface among the low index surfaces, all our calculations were performed on Pd(111) surface.[37] The ideal Pd(111) surfaces were modelled by a 3 × 3 supercell with 5 atomic layers. A lattice constant of 3.904 Å and a k-point grid of 3×3×1 was used. During the optimization process, we relaxed the upper two atomic layers along with the furfural molecule. Bottom three atomic layers were fixed to mimic the bulk of the system. The adsorption energy was calculated using the equation:

$$E_{ad} = E_{Pd(111)+Furfural} - (E_{Pd(111)} + E_{furfural})$$

Where, E_{ad} is the adsorption energy, $E_{Pd(111)+furfural}$ is the energy of the system with furfural molecule adsorbed and $E_{furfural}$ is the energy of the furfural molecule.

Results and Discussion

Characterisation of As-Prepared Catalysts. The experimental conditions at which each 1 wt. % Pd/TiO_2 catalyst was prepared, as well as notation, is presented in table 1, with elemental analysis, by microwave plasma atomic absorption spectroscopy (MP-AES), shown in table S1. The prepared Pd/TiO_2 catalysts were characterized using TEM to assess the particle size distribution (table 1), all images and histograms detailed in the supporting information (figure S1).

Within each solvent environment (A series:H_2O or B series:H_2O/EtOH), decreasing the temperature of preparation, decreases the average Pd particle diameter, in agreement with our previous work with Au based materials.[26] PdA1 (2.5 nm) and PdB1 (1.4 nm) produced the smallest Pd nanoparticles within their respective series, with PdB1 exhibiting the narrowest particle size distribution. It is understood this average particle size is smaller than any previously reported TiO_2 supported Pd metal nanoparticles, synthesized using a PVA/$NaBH_4$ colloidal system.[38] The effect of solvent system can be assessed by comparing samples PdA1 and PdB2, and PdA2 and PdB3, which denote samples prepared at 1°C and 25°C, respectively. Interestingly, the B series of Pd/TiO_2 produces a larger spread of Pd particle size as a function of preparation temperature, with catalyst PdB2 being evidently smaller than the A series equivalent (PdA1). However, the distribution of sizes for the A series is much narrower, and the catalyst prepared at 25°C (PdA2), has a smaller average particle diameter compared to the B series analogue (PdB3). We rationalize these differences by the competing influences during sol-immobilization; the rate of metal precursor reduction, solubility of PVA, and interaction of solvent with the metal salt and formed colloid. PdA1 and PdB1 were examined with HAADF STEM to investigate the presence of Pd clusters that are too small to image clearly with standard TEM (figure 2 and S2). The presence of ultra-small Pd clusters is clearly evident for catalyst PdA1, and are identified by the HAADF STEM images. The ability to achieve significant populations of

Table 1. Solvent and temperature conditions applied for each Pd/TiO_2 catalyst preparation, average Pd particle diameter calculated by TEM analysis and XANES linear combination analysis data for the 1 wt. % Pd/TiO_2 catalysts.

Temperature / °C	H2O/EtOH solvent ratio (vol:vol)	Sample notation	TEM Average Pd diameter / nm	Reference standards (%)		
				Pd^{2+}	Pd^0	R_{factor}
1	100	PdA1	2.5 ± 0.8	33	67	0.043
25	100	PdA2	2.7 ± 0.9	29	71	0.037
50	100	PdA3	2.9 ± 1.5*	20	80	0.036
75	100	PdA4	5.2 ± 2.1*	12	88	0.025
−30	50	PdB1	1.4 ± 0.4	71	29	0.056
1	50	PdB2	2.1 ± 0.6	36	64	0.045
25	50	PdB3	3.4 ± 0.9	25	67	0.043

* As a consequence of dense agglomeration only 100 particles were counted.

metal clusters through standard chemical means remains a challenge, and in accordance with our previous study,[26] we demonstrate how adjusting the temperature of colloidal reduction is able to influence this.

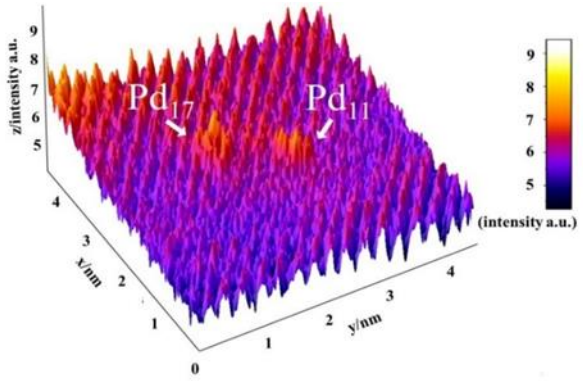

Figure 2. Processed HAADF STEM image of PdA1 showing Pd_{11} and Pd_{17} clusters.

X-ray Absorption Near Edge Structure (XANES) is a valuable tool in probing the speciation of metal nanoparticles, in this instance for determining the Pd oxidation state in the Pd/TiO_2 catalysts under atmospheric conditions (during hydrogenation conditions the oxidic content will reduce to Pd metal). The ratio between Pd^{2+} and Pd^0 was performed by linear combination analysis (LCA) of the 1st derivative of the XANES profile, using PdO and Pd foil as reference standards (table 1 and figure S3). It is evident that for each solvent system, lowering the temperature at which colloidal Pd is prepared results in an increase in Pd^{2+}. All X-ray absorption fine structure (XAFS) measurements represent the whole sample, which means that for NP systems the surface speciation can only influence the overall response for very small NP size; the ratio of surface:core species increases as the average NP diameter decreases. Small Pd NPs form an oxidic surface layer at room temperature when exposed to air,[39] and indeed, we observe a clear correlation between average Pd particle diameter (by TEM) and the extent of Pd^{2+}. The k^2-weighted forward Fourier transform of PdA1 (figure S3) confirms there are no large PdO crystallites. The Pd-Pd scattering path that would otherwise be present at 3Å, and can be observed in the PdO reference, is not observed in the PdA1 data. With this knowledge, it is understandable that the contribution in the PdB1 catalyst is 71% Pd^{2+} and only 29% Pd^0, due to the very small average Pd size in this catalyst. This information, consistent with TEM analysis, confirms that preparing colloidal Pd NPs at a lower temperature results in a decrease in particle size and the formation of clusters. Pd colloidal preparation at −30°C in a mixed $EtOH/H_2O$ solvent shows the most significant interest as the stabilization of ultra-small metal nanoparticles is challenging, but achievable.

To elucidate the specific adsorption sites generated using the different preparation routes, catalysts PdA1, PdA2, PdB1 and PdB2 were evaluated using CO as a probe molecule (figures 3 and S4). Here, the IR frequency of the CO band was used to assess differences in the surface structure of the Pd NPs. The adsorption band present at 2086 cm^{-1}, is assigned to CO linearly adsorbed on corner sites of Pd nanoparticles.[40] There is a secondary linear adsorbed CO band at 2063 cm^{-1}, which can be ascribed to adsorption on Pd nanoparticle edges. Bridge bonded CO can also be identified at ~1975 and 1945 cm^{-1}, with the differences in position attributed to adsorption of facets and edges, respectively.[40] Moreover, there are adsorption bands at 2140, 2120, and 1875 cm^{-1}, assigned to CO adsorbed on Pd^{2+}, Pd^+ and threefold sites, respectively.[41-42] The spectra obtained for all four catalysts exhibit noticeable differences in the distribution of available sites. The relative intensities of the linearly adsorbed CO bands, compared to that from bridge-bonded CO, is much higher for the catalysts prepared in a mixed ethanol-water solvent system. Furthermore, there are differences in the ratio between different types of linear and bridge-bonded sites. The series of NPs prepared in the ethanol water-solvent have a greater proportion of the 2086 cm^{-1} linear adsorbed CO, and 1975 cm^{-1} bridge-bonded CO. It is clear that changing the solvent system of preparation affords Pd NPs with different surface characteristics, most notably the increase in available Pd corner and edge sites. We propose that the different surface sites observed are a consequence of the interaction between the solvent and PVA, which affects the extent of PVA binding on the metal surface.

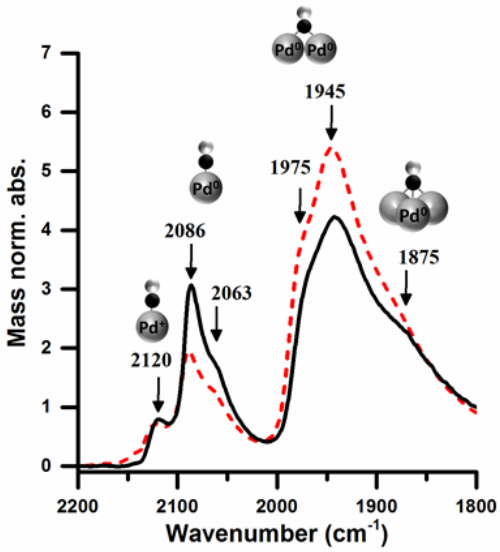

Figure 3. FTIR spectra from CO-adsorption studies on PdB1 (solid black line) and PdA1 (red dashed line).

Catalytic Testing. Both series of catalysts were evaluated for the hydrogenation of furfural (Furfural = 0.3 M; F/metal ratio=500 mol/mol, 5 bar H_2, solvent 2-propanol) at 25°C (table S2) and 50°C (table S3), with the data illustrated graphically in figure 4. Comparing the data between the A series (prepared in water) and B series (prepared in water-ethanol), interesting relationships can be observed. For the A series there is a clear correlation between Pd particle size and activity; smaller Pd NPs are more active, regardless of the reaction temperature. Indeed, the catalyst of the A series of smallest Pd particle size (A1, 2.5 nm), showed the highest catalytic activity (440 and 620 mol (mol Pd)$^{-1}$ h^{-1}, at 25 and 50°C, respectively).

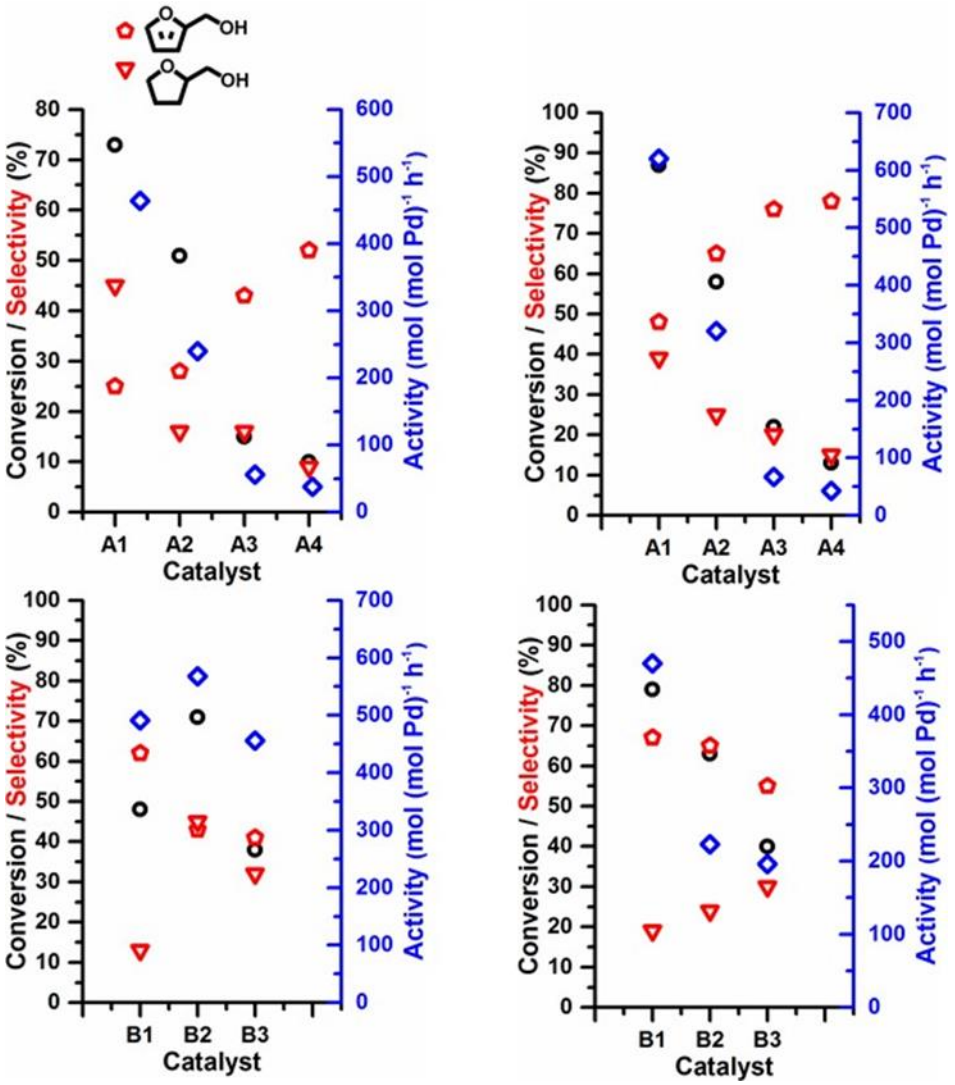

Figure 4. Catalytic performance plots for hydrogenation of furfural using tailored Pd/TiO_2 catalysts (top left) Pd NPs A1→A4 tested at 25°C, (top right) Pd NPs A1→A4 tested at50°C, (bottom left) Pd NPs B1→B3 tested at 25°C, and (bottom right) Pd NPs B1→B3 tested at 50°C. Reaction conditions: Furfural = 0.3 M; F/metal ratio=500 mol/mol, 5 bar H_2, solvent 2-propranol, Converted mol (mol Pd)$^{-1}$ h^{-1} calculated after 15 min of reaction, selectivity calculated at 50% conversion, except catalysts PdA3 and PdA4 at 25°C, where selectivity is calculated at 10% conversion. Open black circles denote conversion. Open blue diamonds denote activity. Red shapes indicate selectivity to the products denoted by the inset key.

For the A series other distinct trends can be seen; as the Pd particle size increases (PdA1 → PdA4), selectivity to furfuryl alcohol increases (48, 65, 76 and 78% for PdA1, PdA2, PdA3 and PdA4, respectively, Table S3) with a decrease in selectivity to tetrahydrofurfuryl alcohol (39, 25, 20 and 15% for PdA1, PdA2, PdA3 and PdA4, respectively, Table S3). On some occasions, the A series catalysts showed improved activity, compared to the B series at comparable particle sizes. Catalyst PdA1, with mean particle size of 2.5 nm has a higher activity at 50 °C than PdB2 (620 and 470 converted mol (mol Pd)$^{-1}$ h^{-1}, respectively, Table S3), despite the smaller particle size of PdB2 (2.1 nm). It must be noted that these Pd mass normalized activities are high when compared against current Pd based catalysts for this reaction.[10, 22] There are clearly other parameters, besides particle size, that influence activity and selectivity, as can be observed by the catalytic performance of the B series. In the case of the B series tested at 25°C, the catalyst, B1 (1.4 nm) was less active than B2 (2.1 nm) with activities of 491 and 568 mol (mol Pd)$^{-1}$ h^{-1}, respectively. The selectivity of B1 is comparable to that of the only previously reported Pd/TiO_2 catalyst (Pd particle also < 2 nm) used for this reaction, despite the different reaction solvent.[17] However, when tested at 50 °C, there was a direct relationship between particle size and activity. Another characteristic difference of the B series is the variation in selectivity profile with increasing particle size. Broadly speaking, there is an inverse relationship for furfuryl alcohol and tetrahydrofurfuryl alcohol selectivity with particle size compared to the A series; as the particle size increases furfuryl alcohol selectivity decreases and tetrahydrofurfuryl alcohol selectivity increases. It is apparent that there is a collaborative effect between the solvent system and temperature of colloidal preparation, which directs the catalytic performance. It is our assertion that the

competing influences of sol immobilization - rate of reduction, PVA solubility, PVA/solvent/colloid interaction – are responsible for the trends observed. The difference in selectivity can be ascribed to the different binding modes of furfural on the Pd surfaces. The CO chemisorption studies for the A and B series show a clear difference in linear CO: bridged CO ratio, with the B series having a far greater proportion of linear sites. Where CO binds linearly to Pd edge and corner sites, previous studies have

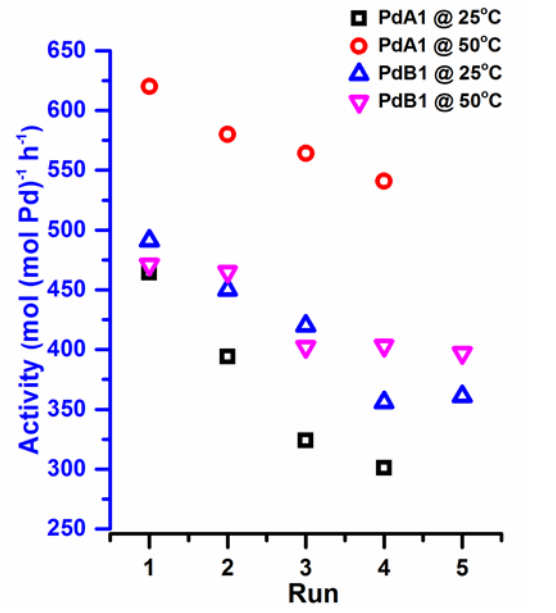

Figure 5. Catalytic activity for Recycling studies of catalysts PdA1 and PdB1.

indicated that these sites tend to bind furfural in a perpendicular orientation, rather than flat across a surface, in agreement with the recent work of Medlin *et al.*[24] In these instances we observe improved selectivity to furfuryl alcohol. Moreover, the adsorption sites that correspond to bridge-bonded or three-fold CO adsorption are able to bind furfural through both the aldehyde functionality and the furan ring and promote the complete reduction to tetrahydrofurfuryl alcohol. Catalysts used for sustainable technologies need to be robust and durable, so recycling studies were performed. The recycling tests were performed on A1 and B1 catalysts at different temperatures (Tables S4 and S5, and figure 5), by reusing the same catalyst without any pretreatment. These data evidenced a significant deactivation of both catalysts when the reaction was performed at 25°C, whereas at 50°C the deactivation was less pronounced. Assessing the reaction profile (Figures S5 and S6) as a function of time, evidences that stronger deactivation phenomena occur for all the catalysts when the reaction was performed at 25°C. To explain the origin of the deactivation the used catalysts were also characterized.

Used Catalyst Characterization. TEM was used to calculate the average Pd particle size after the recycling experiments were performed at both 25 and 50°C. The particle size distribution (figure S7) indicate that for the samples prepared in water, there is a small increase in average size (2.5 to 2.7 nm for PdA1) when performed at 25°C, with no further particle growth when performed at the higher temperature. However, for the Pd catalysts prepared in H_2O:EtOH mixture, the temperature of reaction has a larger influence for PdB1, in which the average particle size increases from 1.4 to 2.0 nm and 2.7 nm when the reaction was performed at 25 and 50°C, respectively and these results are in agreement with the observed initial decrease in catalytic activity. The average Pd particle diameter is still very small and STEM/HAADF was used to identify the presence of Pd clusters in the PdA1 and PdB1 catalysts after performing the reaction at 25°C (figure S8). It is clear that very small Pd clusters are still preserved during catalysis, a combined result of the mild reaction conditions and protective stabilization role of PVA.

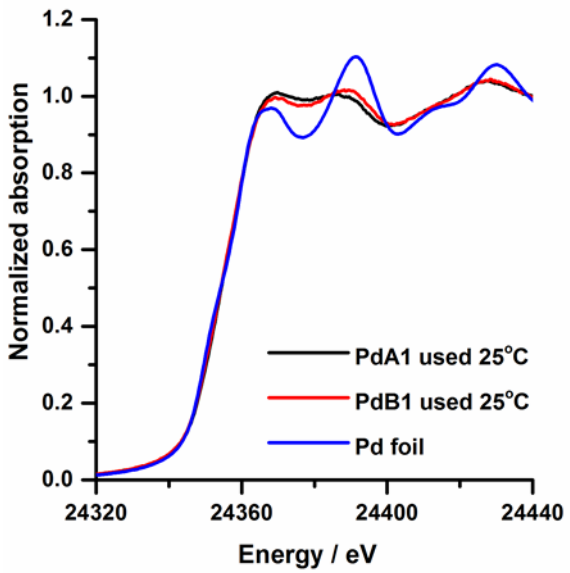

Figure 6. Normalized XANES spectra of PdA1 and PdB1 after catalysis and a Pd^0 reference.

The used PdA1 and PdB1 catalysts tested at 25°C (after 5 reaction cycles) were assessed using XAFS spectroscopy, with the XANES data shown in figure 6. The initial observation from the XANES is the presence of Pd^{2+} and Pd^0. The height of the main edge of the fresh and used catalysts are greater than that of Pd foil. This difference in height can be attributed to the presence of oxidized Pd in the Pd/TiO_2 catalysts. Elsewhere, the maximum of the second XANES peak is seen to move to lower energy for the used catalysts, compared to the Pd foil. The shift in the position of the second maximum is observed for both hydride and carbide forms of Pd, however, the broadening of the first peak is only observed for carbidic Pd.[43-45] In this instance changes in the first peak maximum are complicated by the separate contribution of oxidized forms of Pd. Further evidence of carbide formation was sought by assessing the EXAFS (figures 7 and S9 and table S6), which is able to probe changes in Pd-Pd spacing.

Analysis of the EXAFS data confirms an increase of Pd-Pd spacing after reaction from ~2.74 Å to 2.77 Å. An increase in Pd-Pd spacing is encountered for the formation of Pd carbide and hydride,[39, 46] however, hydride is known to

readily desorb from the Pd lattice under normal atmospheric conditions. Considering this, it is apparent that this expansion could not be caused by the formation of hydride. The expansion of the Pd lattice from 2.74 Å to 2.79 Å has been previously reported for bulk (PdC_x, where x = 0.13) Pd carbide formation, suggesting that only partial carbidization has occurred.[46] We propose that the deactivation encountered at lower reaction temperature is a result of the transformation to Pd carbide, expansion of the Pd-Pd distance, and the subsequent effect on hydrogen dissociation and the η^2 adsorption of C=O and C=C functionalities. Indeed, a greater degree of deactivation is observed for catalysts A1Pd (464 → 394 mol (mol Pd)$^{-1}$ h^{-1}) compared to B1Pd (491 → 450 mol (mol Pd)$^{-1}$ h^{-1}), which correlates with the extent of carbidization observed. Although we experience deactivation upon carbidization, other catalytic processes experience different effects. Previous work investigating the effect of carbide on the catalytic activity of acetylene hydrogenation, concluded that both an increased, or decreased activity can be observed, depending on the type of carbidized Pd site (flat = increase, step = decrease).[47-48]

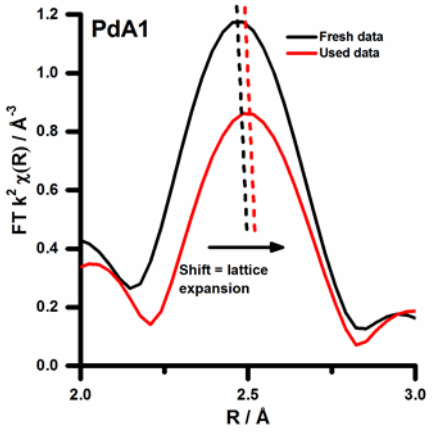

Figure 7. FT χ^2 weighted EXAFS data of fresh (black line) and used (red line) PdA1.

DFT calculations. To assess the effect of carbidization on the adsorption of furfural, DFT calculations were performed. We first considered two different configurations of furfural, parallel and perpendicular, on a pristine Pd(111) surface, (figure 8 (a-b)). In the case of the perpendicular configuration, we considered the stability of the system on top of a Pd atom (Pd_{top}), on the bridge site between two Pd atoms (Pd_{bridge}) and on the three-fold hollow site (Pd_{hollow}). The calculated adsorption energies for the parallel configuration ($Pd_{parallel}$) is -2.160 eV, which is slightly more negative than the earlier reported value of -1.830 eV, which can be accounted for by the different versions of DFT-D approaches used.[21] The adsorption energies for Pd_{top}, Pd_{bridge}, and Pd_{hollow} configurations are -0.632 eV, -0.940 eV and -2.185 eV, respectively, with relaxed structures of Pd_{top} and Pd_{bridge} retaining a perpendicular orientation. However, it is interesting to note that for the Pd_{hollow} site the furfural molecule attained a parallel configuration to the surface after relaxation ($Pd_{hollow\text{-}parallel}$), and is comparable in energy to the $Pd_{parallel}$ configuration. The adsorption energies obtained confirm that the parallel configuration of furfural binding is more stable than the perpendicular orientation. Subsequently, we investigated the increase in Pd–Pd bond distances, as a result of carbidization, in bulk Pd (by 0.095Å) and sub-surface of Pd(111) (by 0.057Å) (Figures S10 and S11), which were consistent with experimentally determined values of partially carbidized Pd nanoparticles.[43-44] We found that the increase in Pd-Pd distance correlated with an increased adsorption energy for furfural. The calculated adsorption energy for this system is -1.613 eV, confirming that adsorption of furfural is more favourable on a pristine Pd(111), compared to a PdC(111). Furthermore, on comparing the geometry of furfural on pristine and carbide systems we find that in both cases parallel adsorption is preferred, although there are some minor differences in the planarity of the furfural adsorption (Table S7).

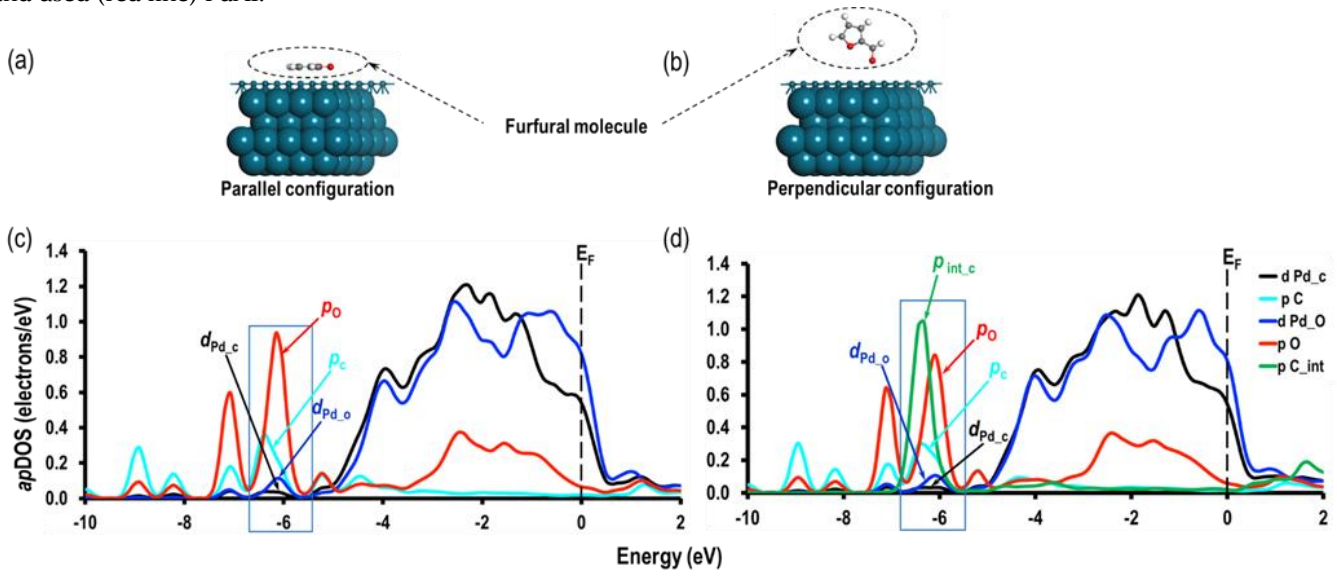

Figure 8 (a) Parallel, (b) Perpendicular configurations of furfural on Pd(111) surface, (c) *ap*DOS for pristine Pd(111) and (d) *ap*DOS for furfural on PdC(111) surface. Black and blue lines represent the signatures for Pd d orbitals close to C and O atoms respectively. Red, aqua and green lines represent the p-orbitals due to C, O and interstitial C atoms respectively.

To assess this change in stability we analyzed the atom projected partial density of states (*ap*PDOS) of the C and O atoms of furfural molecule and Pd atoms of the Pd(111) and PdC(111) surfaces closest to each other. For convenience, the Fermi energy (E_F) is shifted to 0, which is represented by a dotted line in Figure 8 (c-d). From the analysis of *ap*-PDOS we see that around -7.0 eV to -5.5 eV (Figure 8 c-d) there is a strong interaction between the *p*-orbitals, of C and O atoms of furfural, with the *d*-orbital signatures of Pd atoms on Pd(111) surface. However, on incorporating an interstitial C-atom, another sharp signature due to C *p* orbital appears around this region, which has a higher contribution than the *p*-orbital signatures due to C and O atoms of the furfural molecule. The interaction of the C *p*-signatures, due to interstitial C-atoms, interact more strongly with the nearby Pd atoms and result in a weakening of the interaction of furfural C and O atoms with the Pd(111) surface. As a consequence, adsorption of furfural is more favoured on pristine Pd(111), as compared to the PdC(111).

Conclusions.

We demonstrate the tandem optimization of the colloidal preparation of Pd nanoparticles, through adapting a simple and systematic combination of choice of solvent and temperature of reduction. These parameters allow us to tune both the size domains of Pd nanoparticles and available reaction sites, which directs the performance towards the hydrogenation of furfural. Reduced Pd NP size was achieved by lowering the temperature of colloidal reduction; for the catalyst prepared at 1°C in water the average particle size was found to be 2.5 nm, however, we were also able to detect clusters of Pd <20 atoms. For the B series prepared at -30°C, an average particle size of 1.4 nm was produced, which is smaller than has been previously reported for Pd NPs prepared through a PVA/$NaBH_4$ colloidal route. Site selective catalysis was enabled by adjusting the solvent of colloid preparation; the Pd/TiO_2 catalysts prepared using a water-ethanol solvent were found to have a larger proportion of available corner and edge sites, which were able to direct the selectivity of the furfural hydrogenation products. We propose that the greater number of available corner and edge sites adsorb furfural perpendicular to the nanoparticle surface, resulting in greater selectivity to form furfuryl alcohol over the complete reduction product, tetrahydrofurfuryl alcohol. We also find that the selectivity profile does not correspond solely to particle size; for the B series furfuryl alcohol selectivity decreases with increasing particle size, whereas for the A series the inverse relationship is found. The available sites are therefore not just a result of particle size, but also a consequence of the interaction of the protecting agent with the NPs prepared. This influence was also manifested in recycling studies, where those catalysts prepared in water-ethanol, were more robust than those prepared solely in water. By assessing the EXAFS of the used catalysts we were able to identify a Pd-Pd lattice expansion. This is attributed to the formation of Pd carbide, which we propose is responsible for the deactivation observed. This assertion is supported by computational modelling studies, which show the carbidization of Pd, reduces the binding energy of furfural, leading to a lowering of catalytic activity. To our knowledge this is the first report of this proposed deactivation pathway for the hydrogenation α, β-unsaturated aldehydes.

AUTHOR INFORMATION

Corresponding Author

* Email: alberto.villa@unimi.it
* Email: p.p.wells@soton.ac.uk

Author Contributions

S.M.R. synthesized catalysts, performed catalyst characterization (TEM, IR and XAFS) and had major contributions to the writing of the manuscript. M.P. helped to synthesize the catalysts and performed TEM. A.V. and C.E.C.T. conducted all of the liquid phase hydrogenation experiments. N.J. and R.E.P. conducted HAADF STEM. A.C., C.R.A.C., and A.T performed all of the computational studies. N.D and C.R.A.C. were involved in project discussions and supervised the project. P.P.W and A.V. had major contributions to the writing of the manuscript, were involved in all of the project discussions and supervised the project. All authors discussed the results and commented on the manuscript

Funding Sources

The UK Catalysis Hub Consortium is funded by EPSRC (portfolio grants EP I019693, EP/K014706/1, EP/K014668/1, EP/K014854/1 and EP/K014714/1). Via our membership of the UKs HEC Materials Chemistry Consortium, which is funded by EPSRC(EP/L000202), this work used the ARCHER UK National Supercomputing Service.

ASSOCIATED CONTENT

Supporting Information.

TEM HAADF images with supporting Pd particle size distribution histograms, EXAFS fitting parameters, CO-chemisorption IR spectra, micro-wave plasma-atomic emission spectroscopy, computational studies and additional catalytic data for furfural hydrogenation. This material is available free of charge via the Internet at http://pubs.acs.org.

ACKNOWLEDGMENT

The authors wish to acknowledge the Diamond Light Source for provision of beamtime (SP10306). Diamond Light Source are also thanked for the outstanding support of the staff on B18: Prof Andrew Dent, Dr Giannantonio Cibin, Dr Diego Gianolio, Dr Stephen Parry and Mr Phil Robbins. The RCaH are acknowledged for use of facilities and support of their staff. Kristina Penman is thanked for performing the MP-AES measurements. UK Catalysis Hub is kindly thanked for resources and support provided via our membership of the UK Catalysis Hub Consortium.

REFERENCES

1. Hu, X.; Westerhof, R. J. M.; Dong, D.; Wu, L.; Li, C. Z. *ACS Sustain. Chem. Eng.*, **2014**, 2, 2562-2575.
2. Lange, J. P.; Van der Heide, E.; Van Buijtenen, J.; Price, R. *Chemsuschem*, **2012**, 5, 150-166.
3. Huber, G. W.; Iborra, S.; Corma, A. *Chem. Rev.*, **2006**, 106, 4044-4098.

4. Li, G.; Li, N.; Li, S.; Wang, A.; Cong, Y.; Wang, X.; Zhang, T. *Chem. Comm*., **2013**, 49, 5727-5729.
5. Corma, A.; Iborra, S.; Velty, A. *Chem. Rev.,* **2007**, 107, 2411-2502.
6. Yan, K.; Wu, S.; Lafleur, T.; Jarvis, C. *Renew. Sust. Energ. Rev*., **2014**, 38, 663-676.
7. Nakagawa, Y.; Nakazawa, H.; Watanabe, H.; Tomishige, K. *ChemCatChem*, **2012**, 4, 1791-1797.
8. Panagiotopoulou, P.; Vlachos, D. G. *Appl. Catal. A*, **2014**, 480, 17-24.
9. Nakagawa, Y.; Takada, K.; Tamura, M.; Tomishige, K. *ACS Catal.*, **2014**, 4, 2718-2726.
10. Biradar, N. S.; Hengne, A. M.; Birajdar, S. N.; Niphadkar, P. S.; Joshi, P. N.; Rode, C. V. *ACS Sustain. Chem. Eng*., **2014**, 2, 272-281.
11. Rao, R.; Dandekar, A.; Baker, R. T. K.; Vannice, M. A. *J. Catal.*, **1997**, 171, 406-419.
12. Nagaraja, B. M.; Padmasri, A. H.; Raju, B. D.; Rao, K. S. R. *J. Mol. Catal. A: Chem.*, **2007**, 265, 90-97.
13. Rao, R. S.; Baker, R. T. K.; Vannice, M. A. *Catal. Lett*., **1999**, 60, 51-57.
14. Sitthisa, S.; Resasco, D. E. *Catal. Lett.*, **2011**, 141, 784-791.
15. Sitthisa, S.; Sooknoi, T.; Ma, Y.; Balbuena, P. B.; Resasco, D. E. *J. Catal.*, **2011**, 277, 1-13.
16. Sitthisa, S.; An, W.; Resasco, D. E. *J. Catal*., **2011**, 284, 90-101.
17. Aldosari, O. F.; Iqbal, S.; Miedziak, P. J.; Brett, J. L.; Jones, D. R.; Liu, X.; Edwards, J. K.; Morgan, D. J.; Knight, D. K.; Hutchings, G. *J. Catal. Sci. Technol.*, **2016**, 6, 234-242.
18. Iqbal, S.; Liu, X.; Aldosari, O. F.; Miedziak, P. J.; Edwards, J. K.; Brett, J. L.; Akram, A.; King, G. M.; Davies, T. E.; Morgan, D. J.; Knight, D. K.; Hutchings, G, *J. Catal. Sci. Technol.*, **2014**, 4, 2280-2286.
19. King, G. M.; Iqbal, S.; Miedziak, P. J.; Brett, J. L.; Kondrat, S. A.; Yeo, B. R.; Liu, X.; Edwards, J. K.; Morgan, D. J.; Knight, D. K.; Hutchings, G. J. *ChemCatChem*, **2015**, 7, 2122-2129.
20. Shekhar, R.; Barteau, M. A.; Plank, R. V.; Vohs, J. M. *J. Phys. Chem. B*, **1997**, 101, 7939-7951.
21. Vorotnikov, V.; Mpourmpakis, G.; Vlachos, D. G. *ACS Catal.*, **2012**, 2, 2496-2504.
22. Bhogeswararao, S.; Srinivas, D. *J. Catal*., **2015**, 327, 65-77.
23. Schoenbaum, C. A.; Schwartz, D. K.; Medlin, J. W. *Acc. Chem. Res.*, **2014**, 47, 1438-1445.
24. Pang, S. H.; Schoenbaum, C. A.; Schwartz, D. K.; Medlin, J. W. *Nat. Commun*., **2013**, 4, 2448, 1-6.
25. Pang, S. H.; Schoenbaum, C. A.; Schwartz, D. K.; Medlin, J. W. *ACS Catal*., **2014**, 4, 3123-3131.
26. Rogers, S. M.; Catlow, C. R. A.; Chan-Thaw, C. E.; Gianolio, D.; Gibson, E. K.; Gould, A. L.; Jian, N.; Logsdail, A. J.; Palmer, R. E.; Prati, L.; Dimitratos, N.; Villa, A.; Wells, P. P. *ACS Catal*., **2015**, 5, 4377-4384.
27. Wang, Z. W.; Toikkanen, O.; Yin, F.; Li, Z. Y.; Quinn, B. M.; Palmer, R. E. *J. Am. Chem. Soc.*, **2010**, 132, 2854-+
28. Jian, N.; Palmer, R. E. *J. Phys. Chem. C*, **2015**, 119, 11114-11119.
29. Ravel, B.; Newville, M. *J. Synch. Rad*, **2005**, 12, 537-541.
30. Newville, M. *J. Synch. Rad.*, **2001**, 8, 322-324.
31. Grimme, S. *J. Comput. Chem*., **2006**, 27, 1787-1799.
32. Blöchl, P. E. *Phys. Rev. B*, **1994**, 50, 17953-17979.
33. Kresse, G.; Hafner, *J. Phys. Rev. B*, **1994**, 49, 14251-14269.
34. Kresse, G.; Hafner, *J. Phys. Rev. B*, **1993**, 47, 558-561.
35. Kresse, G.; Furthmüller, *J. Phys. Rev. B*, **1996,** 54, 11169-11186.
36. Perdew, J. P.; Burke, K.; Ernzerhof, M. *Phys. Rev. Lett*., **1996**, 77, 3865-3868.
37. Singh-Miller, N. E.; Marzari, N. *Phys. Rev. B*, **2009**, 80, 9.
38. Su, R.; Tiruvalam, R.; He, Q.; Dimitratos, N.; Kesavan, L.; Hammond, C.; Lopez-Sanchez, J. A.; Bechstein, R.; Kiely, C. J.; Hutchings, G. J.; Besenbacher, F. *ACS Nano*, **2012**, 6, 6284-6292.
39. Wells, P. P.; Crabb, E. M.; King, C. R.; Wiltshire, R.; Billsborrow, B.; Thompsett, D.; Russell, A. E. *Phys. Chem. Chem. Phys.*, **2009**, 11, 5773-5781.
40. Lear, T.; Marshall, R.; Lopez-Sanchez, J. A.; Jackson, S. D.; Klapotke, T. M.; Baumer, M.; Rupprechter, G.; Freund, H. J.; Lennon, D. *J. Chem. Phys.*, **2005**, 123, 13.
41. Hadjiivanov, K. I.; Vayssilov, G. N. *Adv. Catal*., **2002**, 47, 307-511.
42. Zhu, H. Q.; Qin, Z. F.; Shan, W. J.; Shen, W. J.; Wang, J. G. *J. Catal*., **2004**, 225, 267-277.
43. Tew, M. W.; Nachtegaal, M.; Janousch, M.; Huthwelker, T.; Van Bokhoven, J. A. *Phys. Chem. Chem. Phys*., **2012**, 14, 5761-5768.
44. McCaulley, J. A. *J. Phys. Chem*., **1993**, 97, 10372-10379.
45. Bugaev, A. L.; Guda, A. A.; Lazzarini, A.; Lomachenko, K. A.; Groppo, E.; Pellegrini, R.; Piovano, A.; Emerich, H.; Soldatov, A. V.; Bugaev, L. A.; Dmitriev, V. P.; Van Bokhoven, J. A; Lamberti, C. *Catal. Today*. **2017**, 283, 119-126.
46. McCaulley, J. A. *Phys. Rev. B*, **1993**, 47, 4873-4879.
47. Yang, B.; Burch, R.; Hardacre, C.; Headdock, G.; Hu, P. *J. Catal.* **2013**, 305, 264-276.
48. Yang, B.; Burch, R.; Hardacre, C.; Hu, P.; Hughes, P. *Surf. Sci.* **2016**, 646, 45-49.

TOC graphic:

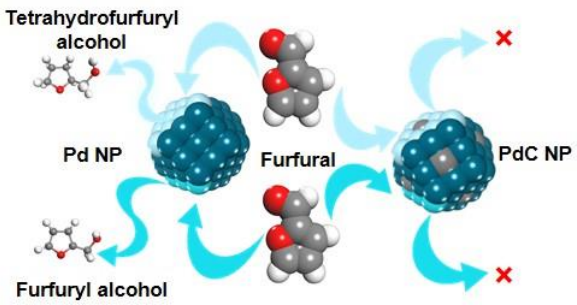
Tetrahydrofurfuryl alcohol
Pd NP
Furfural
PdC NP
Furfuryl alcohol